

Supporting Information

Synthesis and Properties of a POMs-based Trinuclear Copper(II)

Triazole Framework

Li Xu,^a Ying Lu^{a*}, Liping Huang^a, Xiaohui Li^a, Shuang Wang^a, Zhong Zhang^a, Shuxia Liu^{a*}

a. Key Laboratory of Polyoxometalates Science of Ministry of Education, College of Chemistry, Northeast Normal University, Changchun City, Jilin 130024, PR China

Table of Contents

1. Table S1. Crystal data and structural refinement for **1**.
2. Fig. S1 (a) The basic structure of $[\text{Cu}_3(\text{trz})_6(\mu_3\text{-OH})]^{2-}$. (b) The basic structure of $[\text{Mo}_5\text{O}_{18}]^{6-}$.
3. Fig. S2 SEM image of **1**.
4. Fig. S3 Crystal Photograph for **1** under optical microscope.
5. Fig. S4 The FT-IR spectra of **1** from 4000-400 cm^{-1} .
6. Fig. S5 PXRD patterns of solids **1** (black: calculated; red: as-synthesized sample, showing the powder product is in good agreement with the calculated pattern from the single-crystal X-ray diffraction).
7. Fig. S6 The thermogravimetric (TG) curves of **1** measured from 30 to 800 °C under N_2 atmosphere with the heating rate of 10 °C/min.
8. Fig. S7 The thermogravimetric (TG) curves of $\text{K}_3\text{HMo}_5\text{O}_{17}$ measured from 30 to 800 °C under N_2 atmosphere with the heating rate of 10 °C/min.
9. Fig. S8 The thermogravimetric (TG) curves of $\text{Cu}_3(\text{trz})_3(\text{OH})_3(\text{H}_2\text{O})_4$ measured from 30 to 800 °C under N_2 atmosphere with the heating rate of 10 °C/min.
10. Fig. S9 PXRD patterns of $\text{K}_3\text{HMo}_5\text{O}_{17}$ and $\text{Cu}_3(\text{trz})_3(\text{OH})_3(\text{H}_2\text{O})_4$.
11. Fig. S10 UV-vis-NIR absorption spectrum of **1**.
12. Fig. S11 (a) UV-vis-NIR absorption spectrum of $(\text{TBA})_3[\text{Mo}_5\text{O}_{17}\text{H}]$. (b) The diffuse reflectance UV-vis-NIR spectrum of $(Fh\nu)^{0.5}$ vs. energy (eV) for $(\text{TBA})_3[\text{Mo}_5\text{O}_{17}\text{H}]$. (c) UV-vis-NIR absorption spectrum of $\text{Cu}_3(\text{trz})_3(\text{OH})_3(\text{H}_2\text{O})_4$. (d) The diffuse reflectance UV-vis-NIR spectrum of $(Fh\nu)^{0.5}$ vs. energy (eV) for $(\text{TBA})_3[\text{Mo}_5\text{O}_{17}\text{H}]$.
13. Fig. S12 The temperature dependence of the inverse magnetic susceptibility χ_M^{-1} for **1**.
14. Fig. S13 FTIR of Compound **1** after recycling for 5 times.
15. Fig. S14 PXRD patterns of **1** after recycling for 5 times.
16. Fig. S15 Proposed reaction mechanism for the synthesis of cyclohexanone ethylene ketal catalyzed by **1**.

Crystal structure determination

Single crystal XRD analysis of **1** were conducted on a Bruker Smart Apex CCD diffractometer with Mo K α monochromated radiation ($\lambda = 0.71073 \text{ \AA}$) at room temperature. The linear absorption coefficients, scattering factors for the atoms, and anomalous dispersion corrections were taken from the International Tables for X-Ray Crystallography.^[1] Empirical absorption corrections were

applied. The structures were solved by using the direct method and refined through the full matrix least-squares method on F^2 using SHELXS-2014.^[2] Anisotropic thermal parameters were used to refine all non-hydrogen atoms, with the exception for a few oxygen atoms. Those hydrogen atoms attached to lattice water molecules and coordinated water molecules were not located. Crystallization water molecules were estimated by thermogravimetry and only partial oxygen atoms of water molecules were achieved with the X-ray structure analysis. The crystal data and structure refinement results of **1** are summarized in Table S1. Further details on the crystal structure investigation can be obtained free of charge from The Cambridge Crystallographic Data Centre via www.ccdc.cam.ac.uk/data_request/cif on quoting the depository numbers CCDC- 1571612.

Table S1. Crystal data and structural refinement for **1**

Compounds	1
Formula	
Formula weight (g·mol ⁻¹)	1645.46
<i>T</i> (K)	296.15
Wavelength (Å)	0.71073
Crystal system	orthorhombic
Space group	Pbca
<i>a</i> (Å)	17.837(4)
<i>b</i> (Å)	17.886(5)
<i>c</i> (Å)	23.754(6)
α (°)	90
β (°)	90
γ (°)	90
<i>V</i> (Å ³)	7578(3)
<i>Z</i>	8
<i>D</i> _{calc} (mg m ⁻³)	2.884
μ (mm ⁻¹)	4.996
<i>F</i> (000)	6285.0
Crystalsize (mm)	0.21 × 0.2 × 0.19
Goodness-of-fit on F^2	1.054
Final <i>R</i> indices	<i>R</i> ₁ = 0.0815
$[I > 2\sigma(I)]^{[a]}$	<i>wR</i> ₂ = 0.1413
<i>R</i> indices ^[b]	<i>R</i> ₁ = 0.1258
(all data)	<i>wR</i> ₂ = 0.1602

$$^a R_1 = \sum ||F_o| - |F_c|| / \sum |F_o|; ^b wR_2 = [\sum w(F_o^2 - F_c^2)^2 / \sum w(F_o^2)^2]^{1/2}.$$

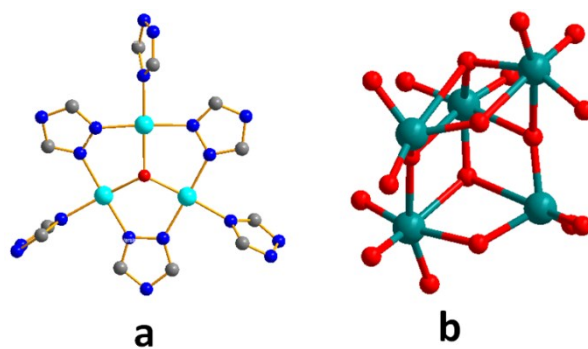


Fig. S1 (a) The basic structure of $[\text{Cu}_3(\text{trz})_6(\mu_3\text{-OH})]^{2-}$. (b) The basic structure of $[\text{Mo}_5\text{O}_{18}]^{6-}$; Color codes: Mo, dark green; O, red spheres; N, blue spheres; C, gray; Cu, light blue.

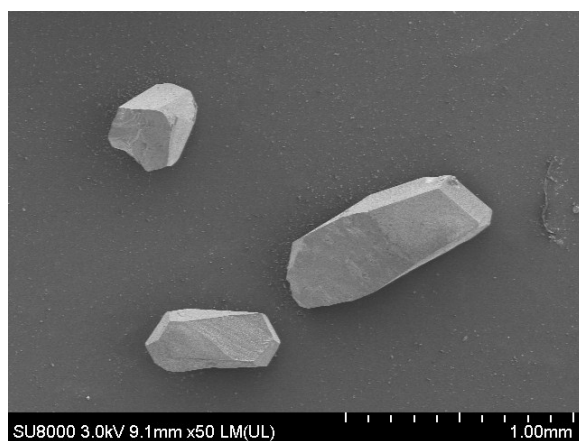


Fig. S2 SEM image of **1**.

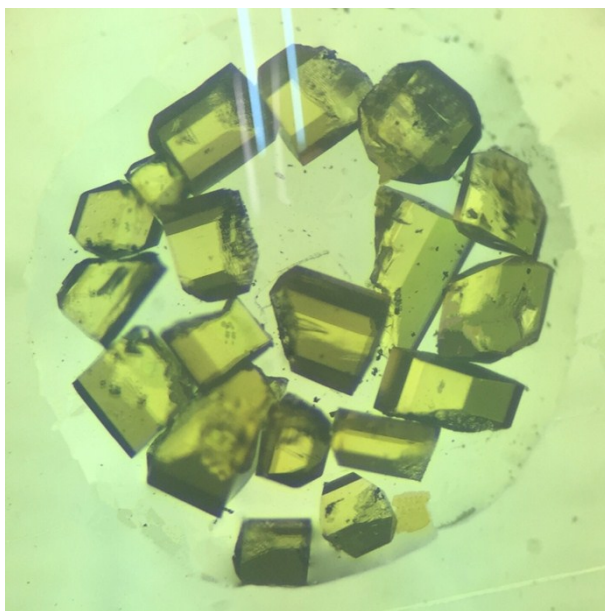


Fig. S3 Crystal Photograph for **1** under optical microscope.

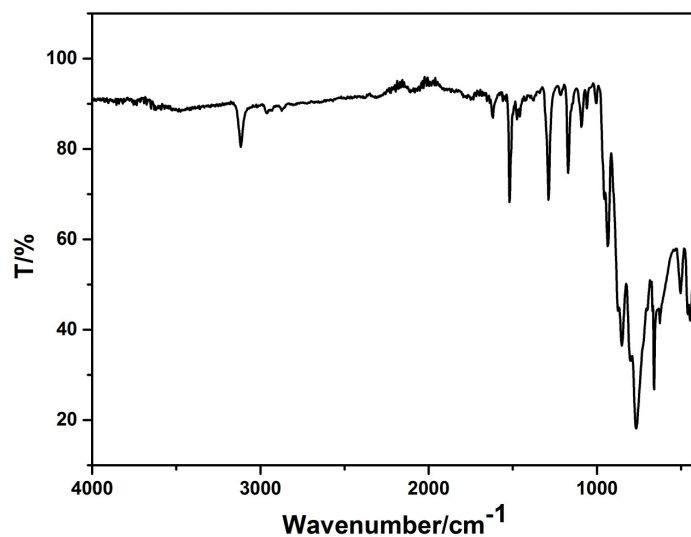


Fig. S4 The FT-IR spectra of **1** from 4000-400 cm^{-1}

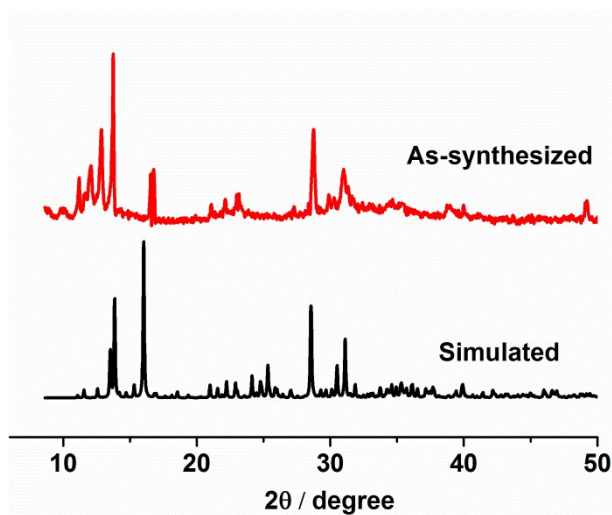


Fig. S5 PXRD patterns of solids **1** (black: calculated; red: as-synthesized sample, showing the powder product is in good agreement with the calculated pattern from the single-crystal X-ray diffraction.

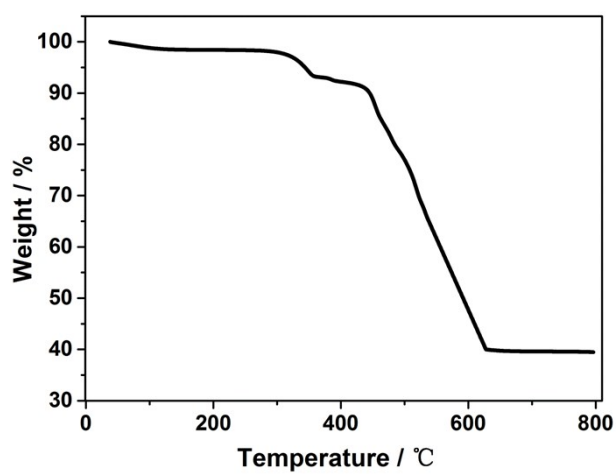


Fig. S6 The thermogravimetric (TG) curves of **1** measured from 30 to 800 °C under N_2 atmosphere with the

heating rate of 10 °C/min.

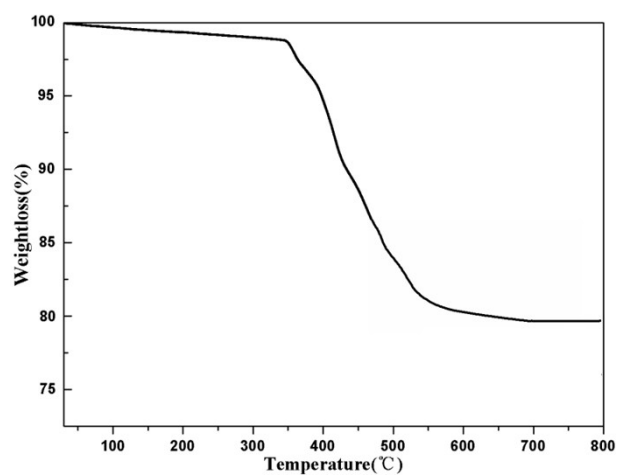


Fig. S7 The thermogravimetric (TG) curves of $K_3HMo_5O_{17}$ measured from 30 to 800 °C under N_2 atmosphere with the heating rate of 10 °C/min.

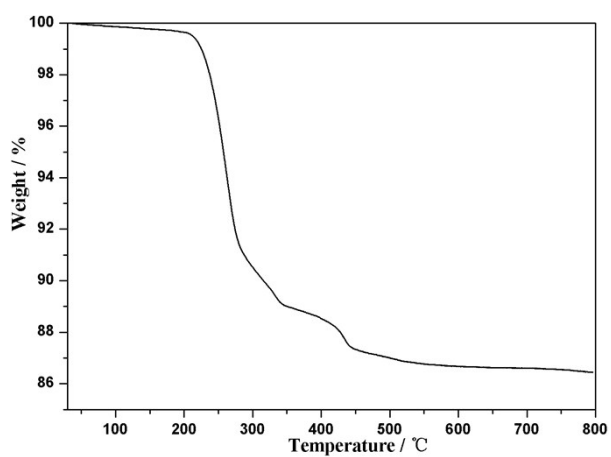


Fig. S8 The thermogravimetric (TG) curves of $Cu_3(trz)_3(OH)_3(H_2O)_4$ measured from 30 to 800 °C under N_2 atmosphere with the heating rate of 10 °C/min.

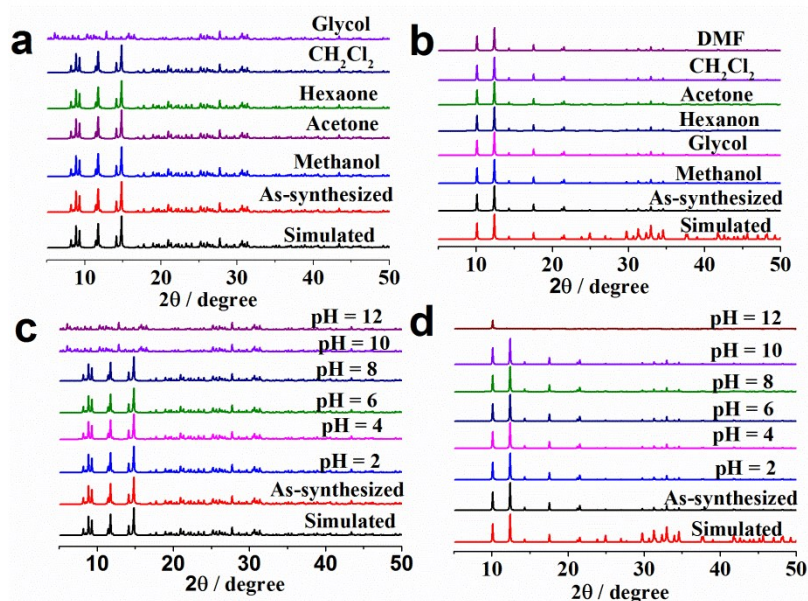


Fig. S9 PXRD patterns of $\text{K}_3\text{HMo}_5\text{O}_{17}$ and $\text{Cu}_3(\text{trz})_3(\text{OH})_3(\text{H}_2\text{O})_4$. (a) The immersion of $\text{K}_3\text{HMo}_5\text{O}_{17}$ in different solvents. (b) The immersion of $\text{Cu}_3(\text{trz})_3(\text{OH})_3(\text{H}_2\text{O})_4$ in different solvents. (c) The immersion of $\text{K}_3\text{HMo}_5\text{O}_{17}$ in aqueous solutions with different pH values. (d) The immersion of $\text{Cu}_3(\text{trz})_3(\text{OH})_3(\text{H}_2\text{O})_4$ in aqueous solutions with different pH values.

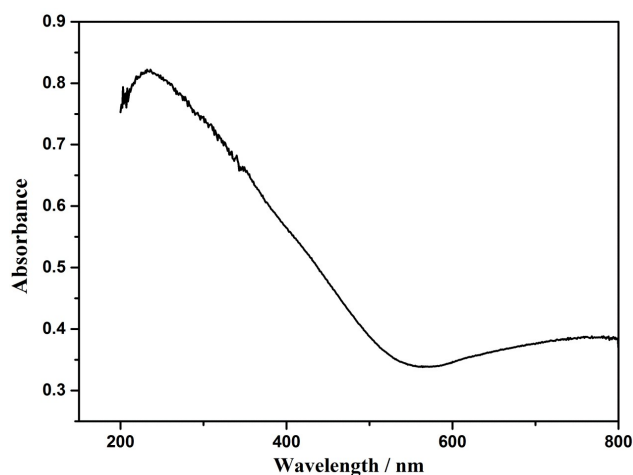


Fig. S10 UV-vis-NIR absorption spectrum of 1.

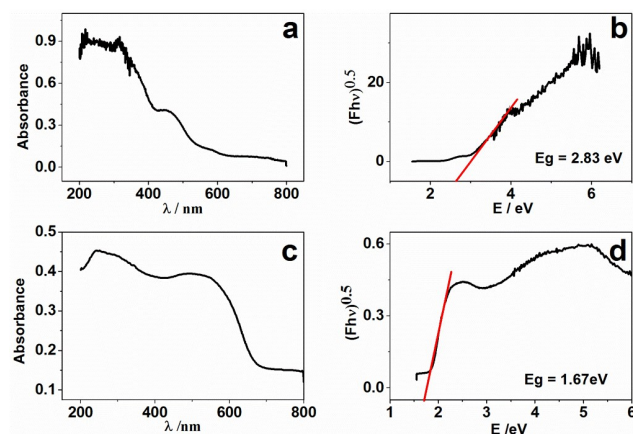


Fig. S11 (a) UV-vis-NIR absorption spectrum of $(\text{TBA})_3[\text{Mo}_5\text{O}_{17}\text{H}]$. (b) The diffuse reflectance UV-vis-NIR spectrum of $(\text{Fhv})^{0.5}$ vs. energy (eV) for $(\text{TBA})_3[\text{Mo}_5\text{O}_{17}\text{H}]$. $F = (1-R) \times (1-R)/2R$; $A = \log 1/R$. (c) UV-vis-NIR absorption spectrum of $\text{Cu}_3(\text{trz})_3(\text{OH})_3(\text{H}_2\text{O})_4$. (d) The diffuse reflectance UV-vis-NIR spectrum of $(\text{Fhv})^{0.5}$ vs. energy (eV) for $(\text{TBA})_3[\text{Mo}_5\text{O}_{17}\text{H}]$. $F = (1-R) \times (1-R)/2R$; $A = \log 1/R$.

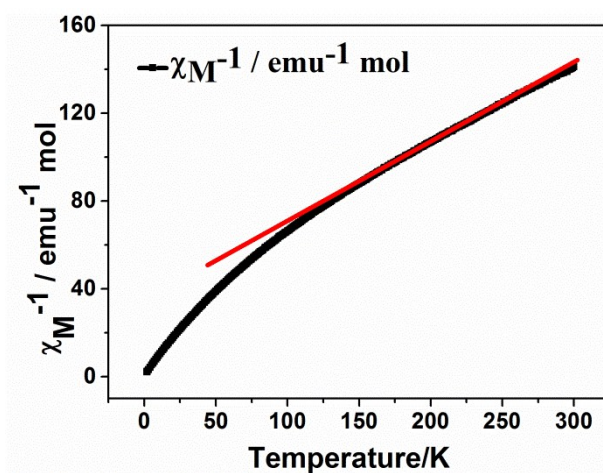


Fig. S12 The temperature dependence of the inverse magnetic susceptibility χ_M^{-1} for **1** at 300 K. The solid red line was generated from the best fit by the Curie-Weiss expression in the range of 48–300 K.

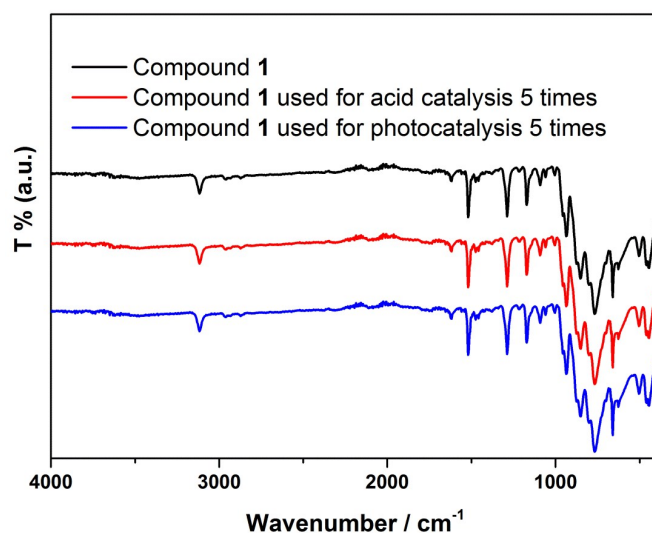


Fig. S13. FTIR of Compound **1** after recycling for 5 times.

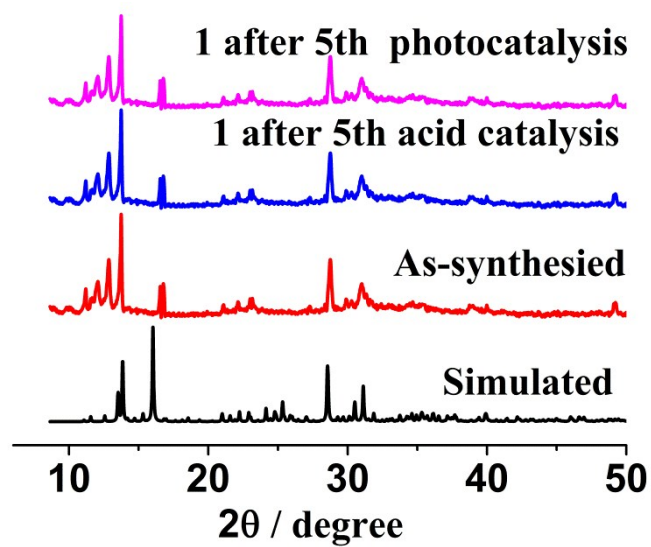


Fig. S14 PXRD patterns of **1** after recycling for 5 times.

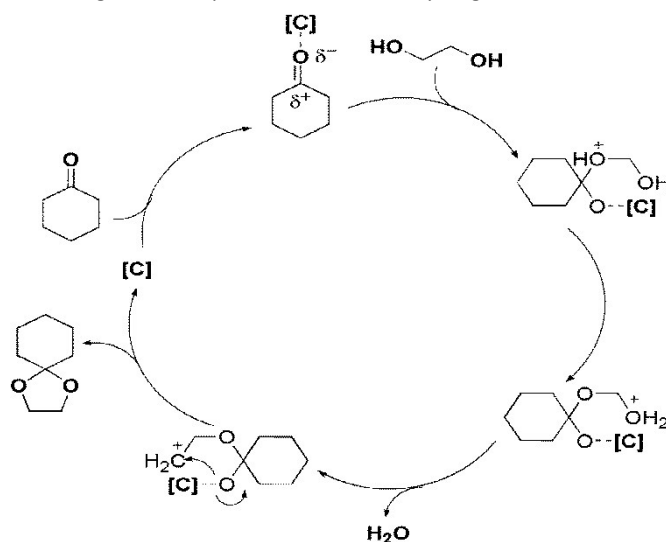


Fig. S15 Proposed reaction mechanism for the synthesis of cyclohexanone ethylene ketal catalyzed by **1**.

References

- [1] International Tables for X-ray Crystallography (Eds.: N. F. M. Henry, K. Lonsdale), Kynoch Press, Birmingham (1952).
- [2] G. M. Sheldrick, SHELXS-2014: Programs for Crystal Structure Solution, University of Göttingen, Göttingen Germany (2014).